Chinese Journal of
POLYMER SCIENCE

RESEARCH ARTICLE

https://doi.org/10.1007/s10118-026-3688-4
Chinese J. Polym. Sci. **2026**, *44*, 3129–3141

Improvements of Hydrophobicity and Toughness of Epoxy Coatings Modified with Hydroxyl-terminated Fluororubber

Yu-Tong Zhou[a], You-Fan Wu[a], Qian-Qian Yang[a], Hai-Bao Zhang[a], Ting Zhang[a*], Hao-Yan Guo[a], Zhen-Jun Wang[a,b*], and Gang Li[c]

[a] *School of Materials Science and Engineering, Chang'an University, Xi'an 710061, China*
[b] *Shaanxi Union Research Center of University and Enterprise for Advanced Transportation Infrastructure Materials, Xi'an 710064, China*
[c] *College of Water Conservancy & Architectural Engineering, Shihezi University, Shihezi 832003, China*

Abstract To address the brittleness of epoxy resin (EP) caused by high crosslinking density, the modification of epoxy resin with flexible rubber segments was proposed in this work. Bisphenol A-type epoxy resin (E51) was reacted with isocyanate-terminated groups *via* an addition reaction to prepare a prepolymer (E51-TDI). Subsequently, E51-TDI was grafted with hydroxyl-terminated fluororubber (HTFR) to synthesize a high-toughness fluorinated epoxy resin (E51-TDI-HTFR) with side chains. A mixture of E51-TDI-HTFR and curing agent (D230) was used to fabricate the coating. The chemical structure of the modified epoxy resin and the thermal, hydrophobic, mechanical, and cavitation erosion resistance of the coatings were investigated. When the HTFR concentration was 25%, the epoxy coating exhibited the best hydrophobicity, mechanical properties, and cavitation resistance. The contact angle of the modified epoxy resin was increased to 110°. Meanwhile, the elongation at break increased to 46.40%, which was approximately four times that of the unmodified coatings. The fracture surface gradually became rougher as the HTFR content increased, indicating a ductile fracture characteristic. Although the addition of HTFR slightly reduced the glass transition temperature, it maintained good thermal stability. In addition, the cavitation erosion resistance of the epoxy coatings was enhanced. This study provides theoretical support for the development of high-toughness and hydrophobic epoxy coatings.

Keywords Epoxy resin; Hydroxyl-terminated fluororubber; Hydrophobicity; Mechanical properties; Cavitation erosion resistance

Citation: Zhou, Y. T.; Wu, Y. F.; Yang, Q. Q.; Zhang, H. B.; Zhang, T.; Guo, H. Y.; Wang, Z. J.; Li, G. Improvements of hydrophobicity and toughness of epoxy coatings modified with hydroxyl-terminated fluororubber. *Chinese J. Polym. Sci.* **2026**, *44*, 3129–3141.

INTRODUCTION

Epoxy resin (EP) has extensive applications in aerospace, automotive, hydraulic structures, and other fields, owing to its mechanical properties, high adhesion, and hydrophobicity.[1–3] However, EP develops a three-dimensional crosslinked network during the curing procedure, resulting in poor toughness and insufficient impact resistance of brittle materials. This brittleness makes coatings susceptible to damage or even delamination when subjected to turbulent impacts, thereby affecting their durability.[4–6] Therefore, the improvement technology of EP toughness has become a key research direction for surface coating materials of hydraulic structures.

Common approaches to enhance the toughness of EP include phase structure modification and interpenetrating network toughening. Phase structure modification is primarily achieved by introducing second-phase materials, such as rubber elastomers,[7] nanoparticles,[8] core-shell polymers,[9] thermoplastic resins,[10,11] and hyperbranched polymers.[12] These materials are incorporated into a crosslinked epoxy network *via* blending to form novel toughening structures. However, this approach often results in uneven dispersion within the curing system owing to the poor compatibility between the second phase and epoxy resin. Therefore, low-molecular-weight liquid rubbers are frequently selected because of their reactive functional groups at both ends and their flexible chain segment structures.[13–15] Rubber can interweave with epoxy resin during the curing process and further induce microphase separation in the epoxy resin,[16,17] enabling the structure to absorb energy and effectively suppress crack propagation, thereby achieving strength enhancement and toughening effects.[18] Chen *et al.*[19] synthesized a PU/EP composite material modified with hydroxyl-terminated liquid nitrile rubber (HTLN) and discovered that adding HTLN improved the toughness of the composite material. Ge *et al.*[20] synthesized polyurethane prepolymers by epoxidizing hydroxyl-terminated polybutadiene (EHTPB) and toluene diisocyanate (TDI) and synthesized modified epoxy resins. Research has found that the toughness, durability, and deformation resistance of epoxy resins can be improved. However, the modified epoxy resin tends to absorb water because of the presence of highly polar cyano groups in nitrile rubber, which is detrimental to its long-term application on hydraulic con-

* Corresponding authors, E-mail: zhangting@chd.edu.cn (T.Z.)
E-mail: zjwang@chd.edu.cn (Z.J.W.)
Received December 11, 2025; Accepted March 27, 2026; Published online June 10, 2026

struction surfaces. Therefore, determining a hydrophobic rubber material with strong environmental adaptability is crucial for the development of surface coatings on hydraulic concrete.

Hydroxyl-terminated fluororubber, as a low-molecular-weight fluorourubber polymer, not only has excellent surface properties and chemical stability but also contains highly reactive functional groups at its end, which can undergo addition reactions with —NCO groups. Therefore, in this study, hydroxyl-terminated fluororubber (HTFR) was chosen to improve the toughness and hydrophobicity of the epoxy resin. Toluene diisocyanate (TDI) was used as a linker to graft flexible fluororubber segments onto the epoxy resin systems. This method effectively absorbs and disperses external stress, thereby improving the impact resistance of the material.[21] Furthermore, owing to the low surface energy of fluorocarbon chains, modified epoxy resins exhibit good hydrophobic properties. This characteristic helps to reduce additional loads and stress concentrations caused by water film formation under flowing water impact conditions, thereby making the modified material more suitable for service requirements in hydraulic structures.[22]

To explore the influence of HTFR on epoxy resin, Bisphenol A-type epoxy resin (E51) and 2,4-toluene diisocyanate (TDI) were used to explore the influence of HTFR on the epoxy resin. Through the addition reactions, E51-TDI was synthesized using E51 and TDI. A high-toughness side-chain fluorinated epoxy resin (E51-TDI-HTFR) was further synthesized using HTFR. Epoxy coatings were prepared by mixing E51-TDI-HTFR with the curing agent D230. A series of characterizations was conducted based on the synthesized materials. The chemical structure of the modified epoxy resin was analyzed. The comprehensive performances of the coatings, including their hydrophobicity, mechanical properties, thermal stability, and cavitation erosion resistance, were evaluated. This work has developed a new technology for preparing epoxy resins with high toughness and hydrophobicity.

MATERIALS AND TEST METHODS

Materials

The raw materials for epoxy coatings included epoxy resin (E51, Guangzhou Suxin Chemical Co., Ltd.), with an epoxy value of 0.54 mol/100g and hydroxyl content of 0.56%; hydroxyl-terminated fluororubber (HTFR, Dongguan Jingbang Polymer Materials Co., Ltd.) having a hydroxyl value of 45 mg KOH/g; 2,4-toluene diisocyanate (TDI, WanHua Chemical Group Co., Ltd.), molecular weight of 174.16, boiling point 251°C at atmospheric pressure; polyetheramine curing agent (D230, Zhongshan Dechuang New Materials Co., Ltd.), total amine content 8.391 meq/g. The EP and HTFR were vacuum-dried for 1 h before use to remove residual moisture from the raw materials.

Sample Preparation

The molar quantity of the hydroxyl groups in HTFR was determined according to the mass ratios of HTFR to E51 (0.15:1, 0.20:1, 0.25:1, and 0.30:1, respectively). The TDI content was calculated based on the 1:1.1 molar ratio between the —OH of HTFR and the —NCO of TDI. The mixing ratios used are listed in Table 1.

Table 1 E51-TDI-HTFR epoxy coatings formulation design.

Group	EP (g)	TDI (g)	HTFR (g)	D230 (g)
HTFR0	100	0	0	33
HTFR15	100	2.31	15	33
HTFR20	100	3.08	20	33
HTFR25	100	3.85	25	33
HTFR30	100	4.62	30	33

E51 was placed in a three-neck flask under a nitrogen atmosphere. Subsequently, the weighed TDI was uniformly added dropwise into the three-neck flask, as shown in Table 1. The mixture was stirred for 30 min and then heated to 60 °C for 2 h. Subsequently, accurately weighed HTFR was added dropwise using a burette. The system temperature was automatically increased to 65 °C for 1 h. The mixture was then further heated to 70 °C and reacted for 2 h, ultimately yielding E51-TDI-HTFR.

Preparation of Epoxy Coatings

According to the ratios shown in Table 1, the curing agents D230 and E51-TDI-HTFR were precisely weighed and thoroughly mixed. After mixing, the sample was subjected to vacuum degassing for 30 min. After casting the final sample into molds, the molds were placed in a vacuum-drying oven. The temperature was gradually increased according to a program of 40, 60, 80, and 100 °C, with each temperature stage curing for 1 h. After the curing schedule was complete, the samples were cooled and demolded. HTFR0 represents the unmodified epoxy coating, whereas HTFR15, HTFR20, HTFR25, and HTFR30 correspond to modified epoxy coatings at different concentrations.

Test Methods

Viscosity

Following GB/T 22314-2008, the viscosities of the samples were determined using a rotational viscometer. Approximately 30 mL of the liquid epoxy resin sample was placed in a temperature-controlled sample holder and maintained at 25 °C for 5 min. Once the reading stabilized, the viscosity value was recorded. The final result was the average of three successive measurements for each sample.

Hydrophobic properties

In accordance with *HG/T 3344-2012*, the water absorption rates of the samples were measured over 2, 4, 6, and 8 days. The contact angles of the samples were determined by applying standard 5 μL of deionized water droplets onto the surface of the sample using the fixed drop technique. Five measurements were systematically taken at different positions on each sample, and the average was calculated to obtain the final static contact angle.

Mechanical properties

(1) Following the standard GB/T 2567-2021, tensile tests were performed at a constant displacement rate of 10 mm/min until the sample fractured. To ensure statistical reliability, three tests were performed for each sample. The stress-strain curves were plotted from the collected tensile data, and Young's modulus was derived from the slope of the initial linear elastic region (0%–0.2% strain) *via* least-squares regression. The average values of the Young's modulus, elongation at break, and tensile strength were reported for subsequent analysis.

(2) The adhesive performances of the samples were evalu-

ated using the ASTM D4541-09. The samples were then evenly applied to the substrates. Subsequently, a 20 mm diameter pull-off pin was firmly attached to the sample-coated surface. After curing, a cutting machine was used to remove the sample from the vicinity of the stud, and the final adhesive strength was reported as the average value of three repeated tests.

(3) Following GB/T 1843-2008, the coating to impact was assessed. The impact strength of the rectangular samples was measured using the instrument display. The final results for each sample are based on the average of three independent tests.

Thermal properties

(1) The thermal characteristics of the samples were analyzed by differential scanning calorimetry (DSC) using a DSC3 instrument. Each sample was enclosed in a standard 40 μL aluminum crucible with a hermetically sealed lid, incorporating a micro-perforation for pressure balance. A controlled heating regimen was applied, increasing the temperature from 50 °C to 150 °C at a rate of 10 °C/min to obtain the DSC results.

(2) Thermogravimetric analysis was performed using a Discovery SDT 650 thermogravimetric analyzer (TGA) to assess the thermal stability and decomposition profile of the sample. Measurements were performed in a flowing high-purity nitrogen environment maintained at 60 mL/min, which served to purge the system and establish inert pyrolysis conditions. The sample was heated from 25 °C to 700 °C at a rate of 10 °C/min. During this process, the mass change was monitored with respect to temperature to obtain thermogravimetric (TGA) and derivative thermogravimetric (DTG) curves.

Cavitation erosion resistance

In accordance with GB/T 6383-2009, cavitation tests were conducted using an XOQ5-1000 ultrasonic material cavitation tester. The upper sample had an end face diameter of (16±0.02) mm and operated at a vibration frequency of 20 kHz. The resin sample served as the lower specimen, fixed on the specimen stage at a distance of (0.5±0.05) mm from the upper specimen and (12±1) mm from the liquid surface. The liquid medium was a 3.5 wt% NaCl solution simulating hydraulic engineering environments. After initial weighing, cavitation and weighing cycles were performed every 30 min, corresponding to cumulative times of 15, 30, 45, and 60 min. At the end of each time point, the following steps were conducted: the samples were removed, wiped clean, then ultrasonically cleaned sequentially with ethanol and deionized water for 2 min each. The samples were then dried in an oven at 40°C for 30 min, cooled to room temperature, and weighed using an analytical balance.

Characterization of E51-TDI-HTFR

The sample structure was characterized using a Fourier transform infrared (FTIR) spectrometer. The spectra were collected in the range of 4000–400 cm^{-1}. The characteristic absorption peak areas were analyzed to investigate the functional group compositions and their changes during the reaction.

Microstructure analyses

(1) The fractured surface morphologies of the coatings were examined using a JEOL JSM-IT800 scanning electron microscope (SEM) operating at an acceleration voltage of 15 kV and ambient temperature (25 °C). Before imaging, the fracture surfaces were carefully cleaned and secured to a specimen holder. The acquired SEM images allowed for a detailed analysis of the fractographic features and investigation of the crack development trajectories.

(2) Laser scanning confocal microscopy (LSCM) was used with a magnification of 5×, scanning frequency of 400 Hz, and image resolution of 1024 dpi × 1024 dpi. The surface morphology of the coating after cavitation erosion was studied over an area of 2566 μm × 2566 μm.

(3) The microphase-separated structure of the sample was characterized using a Nanosurf C3000 atomic force microscope (AFM), with imaging performed over a scan area of 10 μm × 10 μm at a resolution of 512×512 pixels and a scan rate of 1.0 Hz.

RESULTS AND DISCUSSION

Structure and Properties of E51-TDI-HTFR

Structure of E51-TDI-HTFR

Molecular interactions between the fundamental components are shown in Fig. 1. As shown in Figs. 1(a) and 1(d), the peak at 910 cm^{-1} was attributed to the epoxy group in E51, whereas the peak at 2273 cm^{-1} corresponded to the C=O of both the —NCO groups in TDI and the formed isocyanate groups.[23] For TDI, the ratio of the peak area at 2273 cm^{-1} to that of its exclusive skeletal vibration at 1070 cm^{-1} was 50.0. In the spectra of E51-TDI presented in Figs. 1(b) and 1(d), this ratio drastically decreased to 23.1, confirming the consumption of a large number of —NCO groups. The magnitude of this reduction indicates that approximately half of the —NCO groups in the TDI reacted in this step. The appearance of a C=O band at 1731 cm^{-1}, accompanied by the aforementioned reduction at 2273 cm^{-1}, indicates that the —NCO groups in TDI reacted with the —OH groups in EP to form carbamate linkages (—NHCOO—), whereas the epoxy group at 910 cm^{-1} remained unreacted. The ratio of the newly formed C=O band at 1731 cm^{-1} to the epoxy peak area at 910 cm^{-1} at this stage was 0.76.[24] The bands at 1731 and 1110 cm^{-1} were attributed to the C=O and C—O linkages, respectively, of the ethyl acetate solvent in HTFR.

From the spectra of the synthesized E51-TDI-HTFR in Figs. 1(c) and 1(d), the absence of a peak at 1110 cm^{-1} confirms the complete removal of ethyl acetate. Meanwhile, the disappearance of the peak at 2273 cm^{-1} and the enhanced intensity at 1731 cm^{-1} suggest that the —OH groups in HTFR reacted with the residual —NCO groups in E51-TDI, forming additional carbamate linkages.[25] This is quantitatively supported by the increase in the ratio of the C=O peak area to that of the epoxy peak (1731 cm^{-1}/910 cm^{-1}) from 0.76 to 1.88 in the final product, confirming the net formation of additional urethane linkages upon HTFR incorporation.[26] These results collectively confirmed the successful stepwise synthesis of E51-TDI-HTFR with a controlled grafting structure.

Viscosity of E51-TDI-HTFR

The viscosities of the epoxy coatings with different HTFR concentrations are shown in Fig. 2. As shown in Fig. 2, the viscosity of E51-TDI-HTFR gradually increases with increasing HTFR content. As the HTFR concentration was progressively raised from 0 wt% to 30 wt%, the viscosity of the system increased accordingly, from approximately 12.7 Pa·s to 23.9 Pa·s. This phenomenon

https://doi.org/10.1007/s10118-026-3688-4

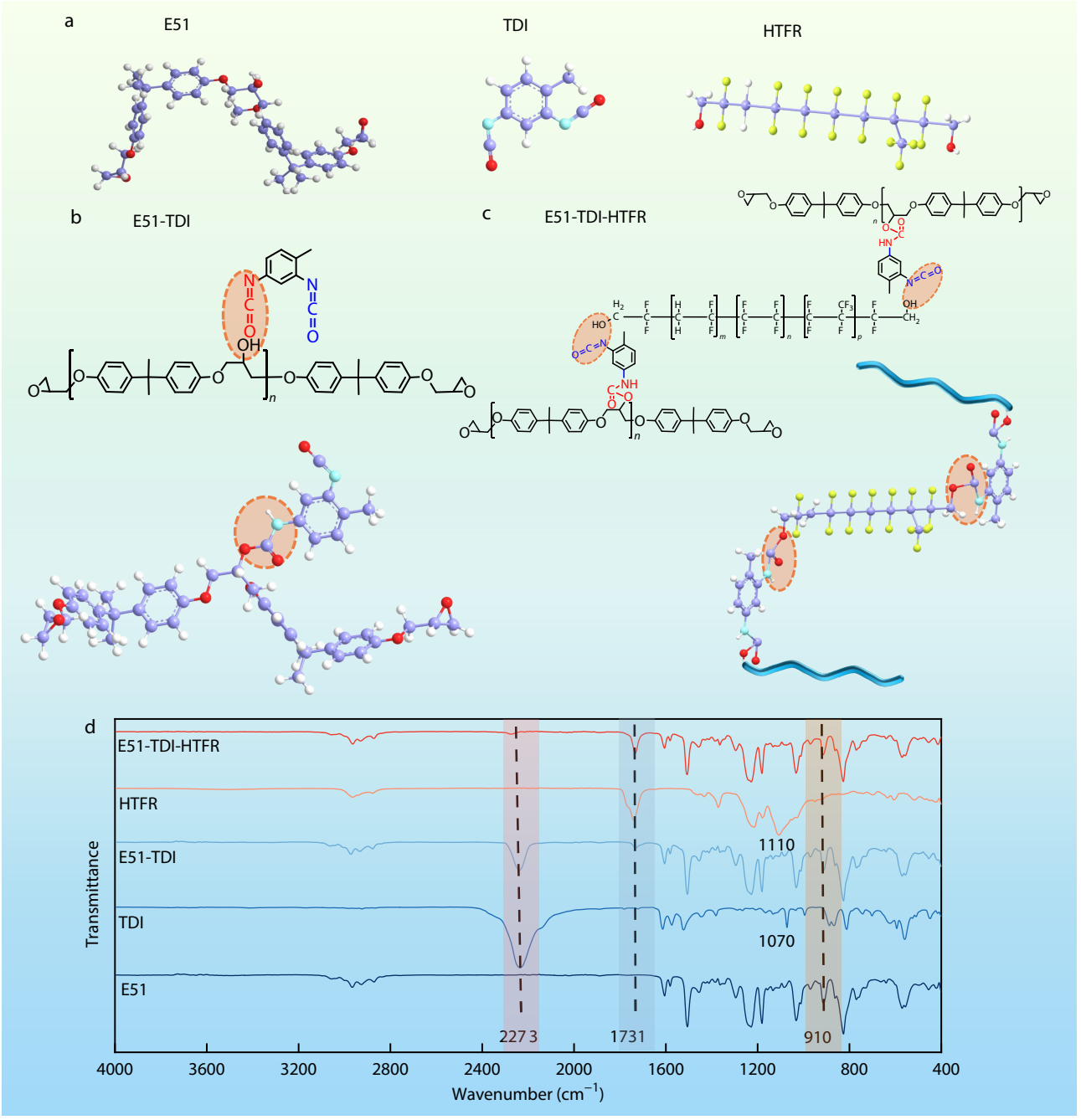

Fig. 1 Molecular interactions among fundamental components: (a) Structure distribution of E51, TDI, and HTFR, (b) Reaction process of E51-TDI, (c) Reaction process of E51-TDI-HTFR and (d) FTIR spectra of the E51-TDI-HTFR synthesis process.

can be attributed to the introduction of long HTFR molecular chains and the formation of chemical bonds, which increase the chain entanglement density with the epoxy matrix and hinder the relative slippage of the molecular chains. Additionally, HTFR itself possesses a high viscosity, and its increasing content contributes to the increase in the viscosity of E51-TDI-HTFR.[27]

Hydrophobic Properties of Epoxy Coatings

Water absorption

The water absorption test results for the epoxy coatings with different concentrations are shown in Fig. 3(a). As the soaking time was increased, the water absorption rate gradually increased. However, compared to HTFR0, the water absorption rate of HTFR25 decreased from 1.66% to 0.67%. This phenomenon is due to the microphase separation caused by HTFR during the curing process of the epoxy resin, in which fluorocarbon chains are dispersed in the epoxy resin in a sea-island structure[28] Compared to unmodified coatings, the movement path of water molecules is prolonged, which hinders their penetration into the resin and prolongs the penetration time[29] However, excessive additive amounts cause surplus rubber to aggregate spontaneously, resulting in severe phase separation. The

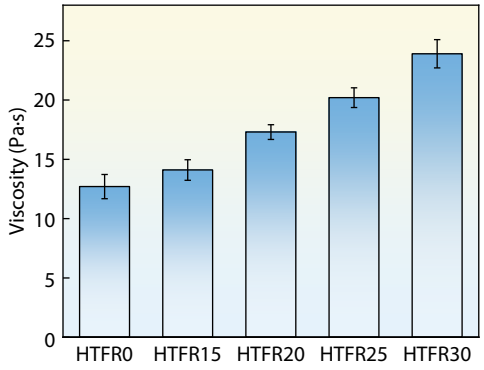

Fig. 2 Viscosity of epoxy coatings at different HTFR concentrations.

resultant interfacial defects created channels that facilitated the penetration of water molecules into the epoxy resin matrix.[30]

Contact angle

The contact angle measurement results for the epoxy coatings with different additive amounts are shown in Fig. 3(b). The contact angle increased from 73° to 110°. This enhancement results from the surface segregation of fluorocarbon chains, which possess extremely low surface energy. These chains migrated to the coating surface and formed a dense hydrophobic layer during curing. This layer repelled water and promoted the formation of spherical droplets. However, the contact angle decreased when the additive content reached 30%. This decrease was due to the excessive aggregation of the hydroxyl-terminated fluororubber, resulting in severe phase separation. Therefore, high-surface-energy epoxy resins are exposed because of the generation of microcracks and voids at the interface, leading to weakening of the hydrophobic effect.[31,32]

Mechanical Properties of Epoxy Coatings

Tensile properties of epoxy coatings

The mechanical properties of epoxy coatings with different HTFR concentrations are shown in Fig. 4. As shown in Figs. 4(a) and 4(b), the Young's modulus of HTFR0 is approximately 1.16 GPa, exhibiting high rigidity and brittleness, with almost no plastic deformation before fracture. With the addition of the HTFR, a preliminary "sea-island structure" forms within the material, which can induce crazing and shear bands, thereby achieving toughening. For HTFR25, the modulus decreased moderately to approximately 0.67 GPa. The formation of a microphase-separated structure with an appropriate domain size and strong interface can consistently trigger shear yielding of the epoxy matrix during deformation, resulting in a broad and high stress plateau.[33] However, when the addition amount reaches 30%, the excessive rubber phase led to a sharp decrease in the material's Young's modulus to about 0.12 GPa and a significant reduction in strength. Although the ductility was further improved, its load-bearing capacity was severely compromised, failing to satisfy its strength.[34]

As shown in Fig. 4(c), HTFR0 exhibited high tensile strength and low elongation at break. After the HTFR modification, the tensile strength of the epoxy coatings decreased slightly, whereas the elongation at break increased significantly. Specifically, the tensile stress decreases to 21.98 MPa with a about additive content, whereas the elongation at break improved remarkably to 46.40%. This phenomenon can be attributed to two factors, as shown in Fig. 4(f). First, the unmodified epoxy coating possessed a highly crosslinked network. In contrast, the modified system introduced long flexible segments through the reaction between the hydroxyl group at the end of the HTFR and the —NCO group in TDI, forming amino ester bonds with a bridge-like structure. A microphase-separated structure is formed during curing, which effectively absorbs energy through a pinning mechanism during tensile deformation. Second, the inherent flexibility of fluorocarbon chains allows for greater deformation under stress, thereby enhancing the toughness of the coating. However, because the HTFR phase has a substantially lower elastic modulus than the epoxy resin, it is preferentially destroyed under stress, resulting in a slight decrease in the tensile strength relative to the unmodified coating.[35]

When the HTFR content reached 30%, the tensile strength decreased significantly, and the elongation at break increased abnormally. This decline was due to the spontaneous aggregation of excess HTFR, which led to the formation of oversized particles and excessive phase separation. Therefore, an excessively large loose area was formed, leading to the generation and rapid propagation of microcracks.[36]

Impact properties of epoxy coatings

As shown in Fig. 4(d), HTFR0 exhibits an impact strength of 10.42 kJ/m^2. At 25% additive content, the impact strength reaches 24.53 kJ/m^2. This improvement is due to the role of TDI

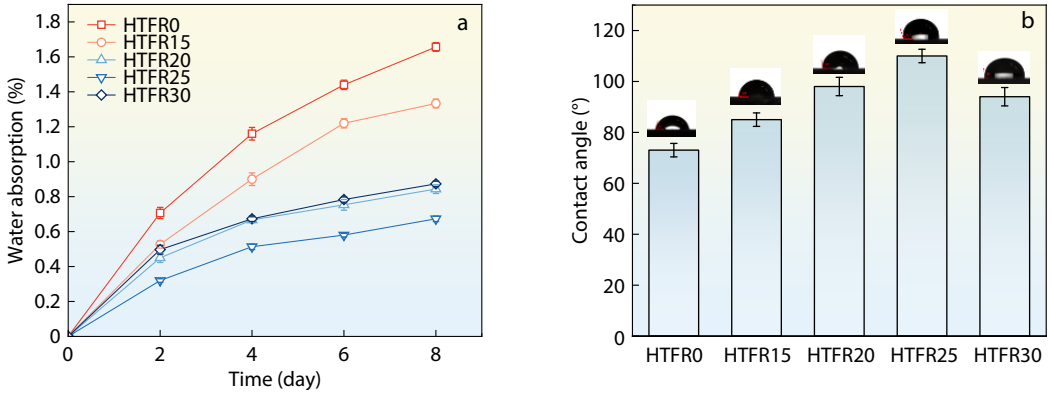

Fig. 3 Hydrophobic properties of epoxy coatings at different HTFR concentrations: (a) water absorption, (b) contact angle.

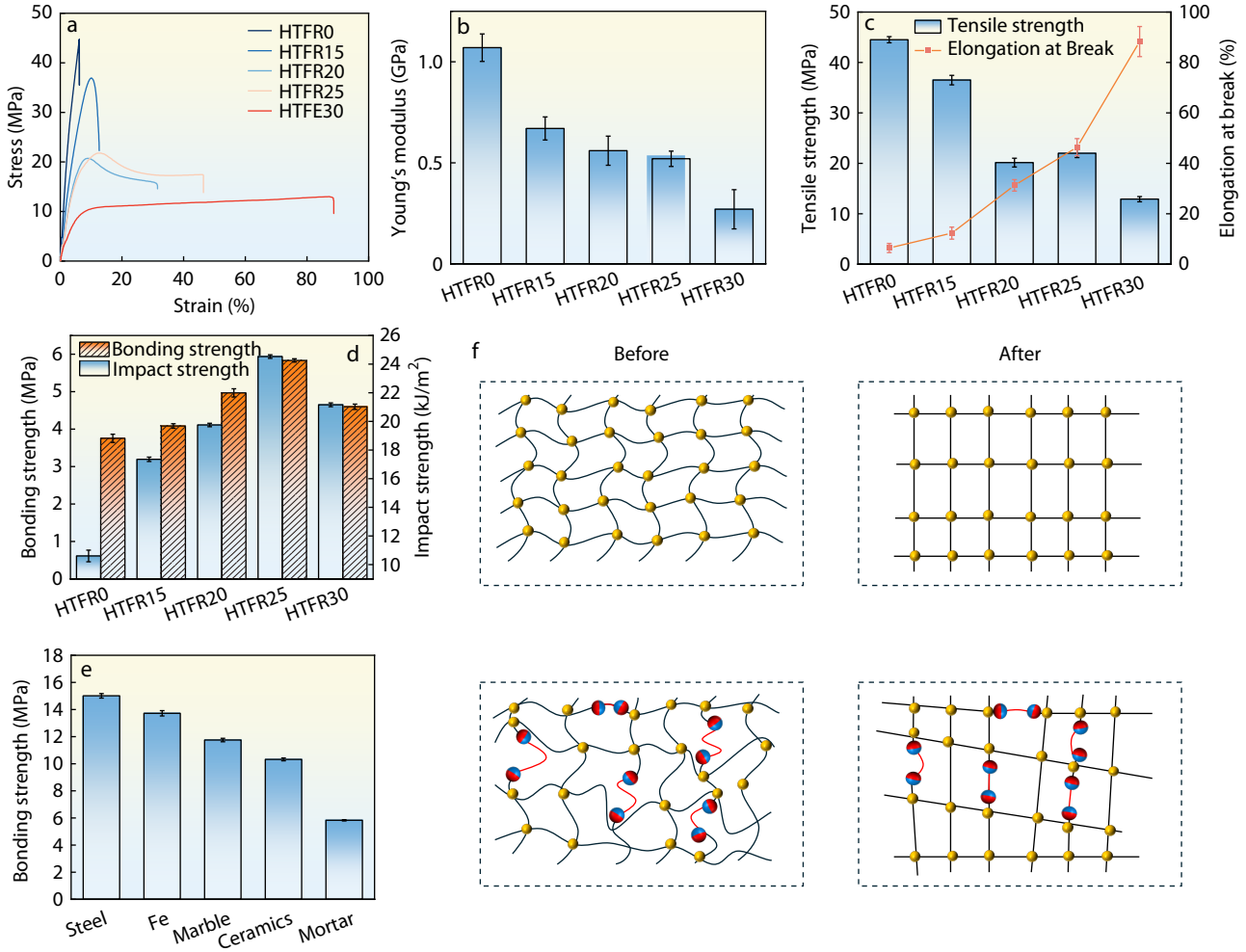

Fig. 4 Mechanical properties of epoxy coatings with different HTFR concentrations: (a) stress-strain curve, (b) Young's modulus, (c) elongation at break and tensile stress, (d) impact strength and bonding strength, (e) bonding strength of HTFR25 on different substrates, (f) schematic of mechanism enhancing mechanical properties.

as a crosslinking agent, which forms amino ester bonds to connect the epoxy resin with HTFR, thereby enhancing the binding force between the epoxy resin and HTFR. Furthermore, HTFR was distributed as a microphase within the epoxy. When the coating is subjected to impact, the HTFR particles initiate the formation of shear bands, absorbing substantial energy. This mechanism effectively suppresses crack initiation, thereby improving impact resistance. However, at an additive content of 30%, excessive HTFR agglomerated into large second-phase particles. Upon impact, cracks preferentially initiated at these agglomerates and propagated through the matrix. Simultaneously, the excess HTFR reduces the crosslinking density of the epoxy, decreasing its rigidity and compromising its impact properties. Despite this decline, all modified formulations exhibited higher impact strengths than the unmodified system.[37]

Bonding properties of epoxy coatings

As shown in Fig. 4(d), the bonding strength between the epoxy coatings and mortar substrates exhibited significant concentration-dependent behavior with varying HTFR concentrations. For the pure epoxy coating without HTFR modification, the interfacial bonding strength with the mortar was measured as 3.75 MPa. As the HTFR concentration increased, the bonding strength exhibited a clear upward trend. When the HTFR addition reached the optimal level, the bonding strength rises to 5.83 MPa, representing an improvement of approximately 55.5% compared to the unmodified system. This enhancement can be attributed to the role of TDI as an effective coupling agent at lower incorporation levels, which establishes robust chemical bonding interfaces between the HTFR rubber and epoxy resin. Consequently, strong interfacial bonding enhances bond strength by efficiently transferring stress from the rigid epoxy matrix to the flexible rubber phase and suppressing early failure modes, such as interfacial debonding.

However, when the HTFR content exceeded the optimal value, the bonding strength decreases to 4.59 MPa. This decline occurred because excessive rubber content led to local aggregation of the rubber phase, resulting in higher stress concentrations at the interface. These stress concentrations served as preferential sites for crack initiation and propagation. Moreover, an excessively high rubber content substantially reduces the overall modulus of the material. An excessively compliant matrix cannot effectively support the stress transferred through the interface, ultimately leading to a re-

duction in bonding strength.[38]

As shown in Fig. 4(e), HTFR25 demonstrated excellent bonding performance across a variety of substrates. Its bonding strength reaches 15.01 MPa on stainless steel and 13.72 MPa on iron-based surfaces. For nonmetallic inorganic materials, HTFR25 achieves strengths of 11.75 MPa on marble and 10.32 MPa on ceramic. Even on the porous and relatively weak mortar substrate, the bonding strength remains notably high at 5.83 MPa. These results collectively confirm that HTFR25 possesses a strong and versatile adaptability to different types of substrates, indicating its outstanding comprehensive bonding performance.[39]

Thermal Stability of Epoxy Coatings

DSC analysis

The thermal degradation behavior of the epoxy coatings with different HTFR concentrations is shown in Fig. 5. As shown in Figs. 5(a) and 5(b), the glass transition temperature (T_g) of the coatings decreases with increasing HTFR content. HTFR0 exhibits a T_g of 74.3 °C, but the T_g of HTFR30 is 65.8 °C. The introduction of flexible carbon chain side groups increased the spacing between crosslinking points and significantly increased the free volume of the cured system.[40] Furthermore, hydroxy-terminated liquid fluororubbers contain numerous fluorocarbon segments, which are characterized by low internal rotational resistance and high molecular mobility. Therefore, the modified epoxy coating became more susceptible to segmental movement when heated, leading to a lower T_g.[41]

Thermodynamic analysis indicated that the decrease in T_g demonstrated that the incorporation of flexible segments increased the free volume, enabling easier molecular movement under stress. Therefore, plastic deformation can be induced to dissipate energy, thereby significantly improving the toughness of the epoxy coatings. This enhancement in toughness was achieved while maintaining adequate thermal stability for practical applications. Although T_g progressively decreased with increasing HTFR content, all the modified epoxy resins maintained T_g values higher than room temperature, satisfying the application requirements.

TGA analysis

The TGA/DTG results for HTFR0 and HTFR25 are shown in Figs. 5(c) and 5(d), respectively. By comparing the TGA results, it was found that E51 had the same thermal weight loss stage before and after modification, indicating good compatibility between HTFR and E51.[42,43] The DTG result for HTFR0 shows a sharp single peak, indicating that the chain segments of the epoxy resin break rapidly after reaching the highest decomposition temperature. In contrast, the main peak width in the HTFR25 DTG results significantly increased, and the peak shape was relatively flat, indicating that the heat resistance of the epoxy resin with added HTFR was slightly reduced compared with that before modification. Owing to the addition of HTFR, the crosslinking density of the epoxy resin was reduced, resulting in a slight decrease in its thermal stability.[44]

Cavitation Erosion Resistance of Epoxy Coatings

Mass loss of epoxy coatings after cavitation erosion

The cavitation erosion resistance of epoxy coatings with different HTFR concentrations is shown in Fig. 6. As shown in Fig. 6(a). The cumulative mass loss for all the samples increased with pro-

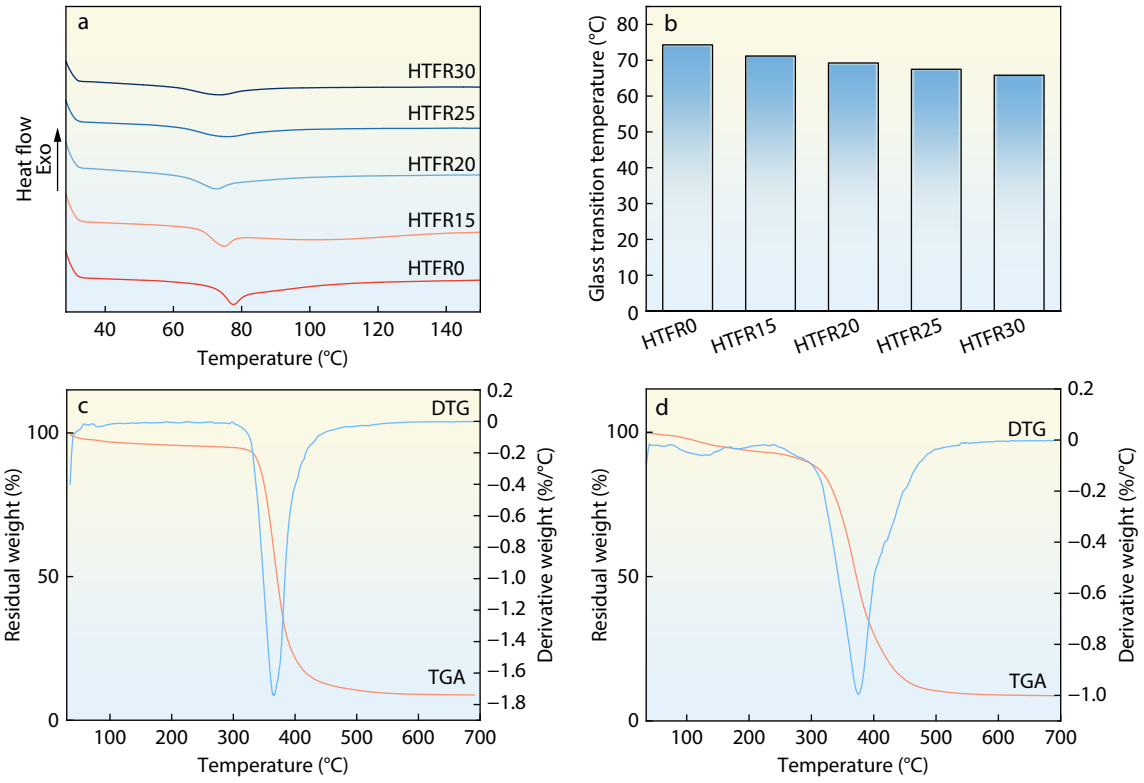

Fig. 5 Thermal degradation behavior of epoxy coatings with different HTFR concentrations: (a) DSC results, (b) glass transition temperatures, (c) TGA and DTA results of HTFR0, (d) TGA and DTA results of HTFR25.

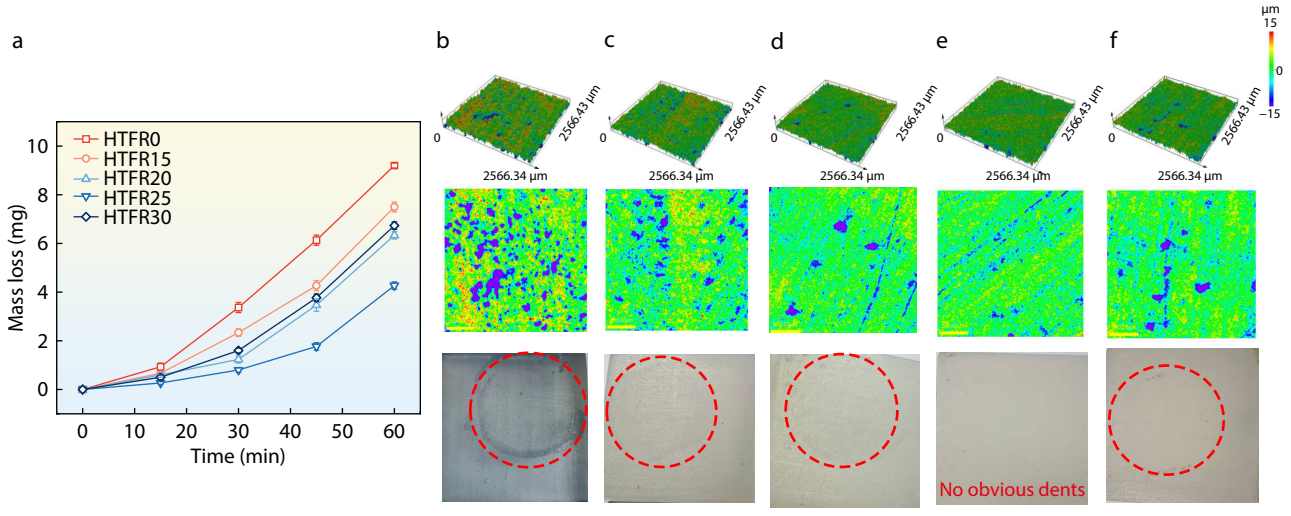

Fig. 6 Cavitation erosion resistance of epoxy coatings with different HTFR concentrations: (a) cavitation mass loss, (b) HTFR0, (c) HTFR15, (d) HTFR20, (e) HTFR25, (f) HTFR30 morphological changes after cavitation.

longed exposure time. After 60 min, the coating with 25% HTFR showed a cumulative mass loss of only 4.2 mg, whereas that of the unmodified epoxy resin reaches 9.2 mg.

This improvement results from the ability of the fluorocarbon segments to induce crazing under the impact of shock waves and microjets from collapsing bubbles, thereby absorbing and dissipating energy. Consequently, when cavitation bubbles impact the coating, stress is effectively transferred from the epoxy resin to the rubber phase, reducing mass loss. Furthermore, the low surface energy of fluorine atoms in the HTFR enhances the overall hydrophobicity of the coating, which helps prevent water penetration into defects and delays mass loss.[45]

However, at 30% additive content, excessive HTFR led to poor dispersion and severe phase separation within the epoxy resin. This results in the formation of oversized, loose-phase regions that are highly susceptible to damage during bubble collapse, thereby accelerating the mass loss rate. Compared to unmodified epoxy coatings, the incorporation of flexible segments endows epoxy coatings with improved toughness and hydrophobicity, thereby significantly enhancing their resistance to cavitation erosion in water.[46]

Morphology of epoxy coatings after cavitation erosion

The cavitation erosion resistance of the epoxy coatings with different additive amounts is shown in Figs. 6(b)–6(f). Warm colors correspond to surface protrusions, whereas cool colors represent cavitation pits. As shown in Fig. 6(b), the most severe cavitation damage occurs in the unmodified epoxy coating, which exhibits numerous pits. This phenomenon is attributed to the brittle network of the coating, which cannot effectively dissipate the impact energy of bubbles. Direct breakage of the epoxy molecular chains led to rapid crack propagation.

As shown in Figs. 6(c)–6(e), the number of cavitation pits gradually decreases with increasing HTFR content. This improvement occurred because the flexible segments acted as stress concentrators, inducing numerous crazing and plastic deformations that consumed most of the impact energy. Furthermore, the extremely low surface energy of fluorocarbon chains effectively prevents water penetration into cracks and pores, thereby inhibiting further deterioration from moisture infiltration. The combined toughness and hydrophobicity of the modified coating significantly improve its cavitation erosion resistance, resulting in smoother surfaces after testing.

As shown in Fig. 6(f), excessive additive amounts excessively diluted the rigid epoxy network and substantially reduced the crosslinking density. Therefore, the resistance of the coating to the cavitation impact is compromised. Additionally, the severe phase separation caused by HTFR aggregation creates defects and stress concentration points, making the coating more susceptible to damage.[47]

Morphology and Toughening Mechanism of Epoxy Coatings

Morphology of epoxy coatings after fracture

The morphologies of the epoxy coatings with different HTFR concentrations after fracture are shown in Fig. 7. In Fig. 7(a), the fracture surface of the unmodified epoxy resin appears relatively smooth and displays numerous clear regular cracks without noticeable branching or deflection, indicating typical brittle fracture characteristics.[48] As shown in Figs. 7(b) and 7(c), the fracture surfaces became progressively rougher with increasing HTFR content, exhibiting distinct dimples and hook-like structures that demonstrate ductile fracture behavior. This transformation results from the formation of a microphase-separated structure during curing, which effectively absorbs energy through a pinning mechanism during tensile deformation.[49] In Fig. 7(d), the coating with 25% HTFR displays a high density of vortex-like cracks on its fracture surface, providing direct evidence of substantial energy dissipation during failure and confirming the effectiveness of HTFR in enhancing the toughness. However, as shown in Fig. 7(e), excessive HTFR addition reduced the number of induced cracks, consequently diminishing the toughening effect.[50]

The phase structure of epoxy coatings

The phase structures of the epoxy coatings with different HTFR concentrations are shown in Fig. 8, where the bright regions correspond to the soft HTFR rubber phase, and the dark regions

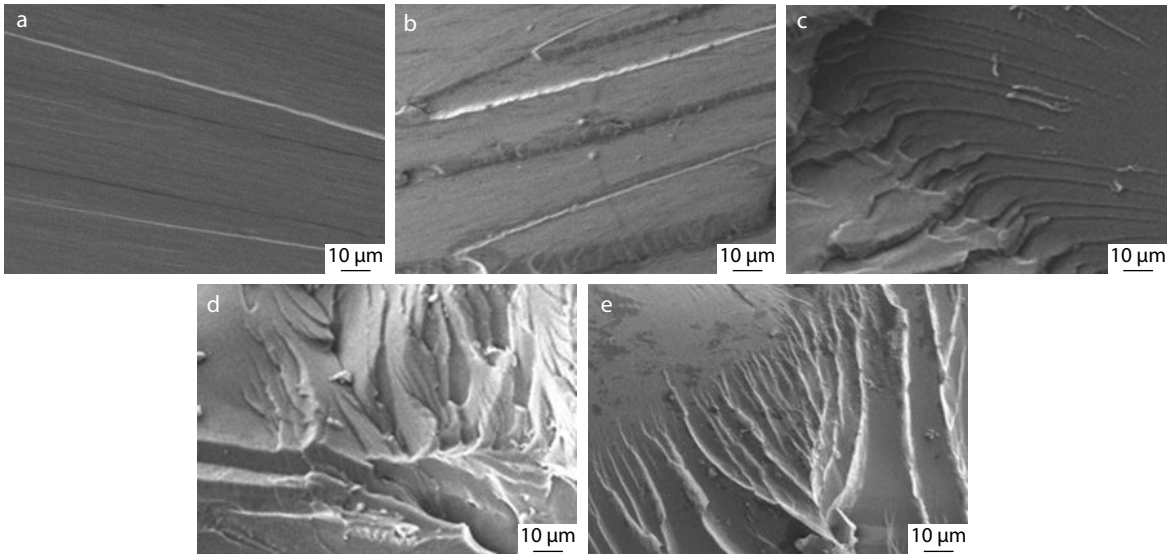

Fig. 7 Morphology of fracture surfaces of epoxy coatings with different HTFR concentrations: (a) HTFR0, (b) HTFR15, (c) HTFR20, (d) HTFR25, (e) HTFR30.

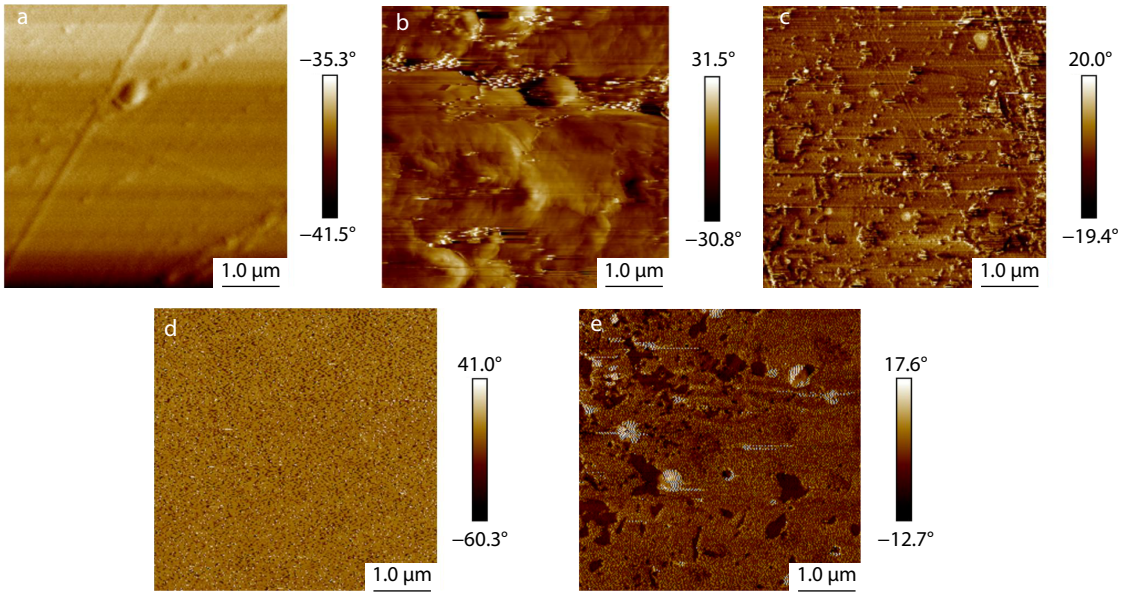

Fig. 8 The phase structures of epoxy coatings with different HTFR concentrations: (a) HTFR0, (b) HTFR15, (c) HTFR20, (d) HTFR25, (e) HTFR30.

correspond to the rigid epoxy resin matrix. It can be observed from the figure that as the HTFR content increases, the rubber phase transitions from locally aggregated domains to a more uniformly dispersed state. At an addition level of 25%, the rubber phase exhibited a moderate domain size and uniform distribution within the epoxy matrix with clear interfacial boundaries between the two phases, resulting in a well-defined microphase-separated structure.[51,52] In contrast, an excessively high HTFR content leads to severe aggregation of the rubber phase, coarsening of the domains, and blurred interfaces, thereby introducing stress concentration defects and compromising the overall performance of the material.[53]

Synthetic reaction mechanism of E51-TDI-HTFR

The toughening mechanism of epoxy coatings modified with HTFR is illustrated in Fig. 9. In the first stage, the —OH groups of epoxy resin E51 reacted with the 4-position —NCO groups of TDI. The hyperconjugation and inductive effects of the methyl group on the benzene ring confer higher electrophilicity and reactivity to the 4-position —NCO groups. Consequently, these groups preferentially reacted with E51 to achieve successful grafting. In the second stage, the terminal —OH groups of HTFR reacted with the remaining 2-position —NCO groups of TDI. After the reaction temperature was elevated, the less reactive 2-position —NCO groups subsequently reacted with the HTFR, thereby connecting E51 with the HTFR. In the third stage, a crosslinked network structure formed after the addition of the curing agent D230 to the modified epoxy resin. By adding flexible HTFR segments, the spacing between the crosslinking points in the epoxy resin increases, resulting in reduced crosslinking density and consequently enhanced mobility of the molecular chains.[54]

https://doi.org/10.1007/s10118-026-3688-4

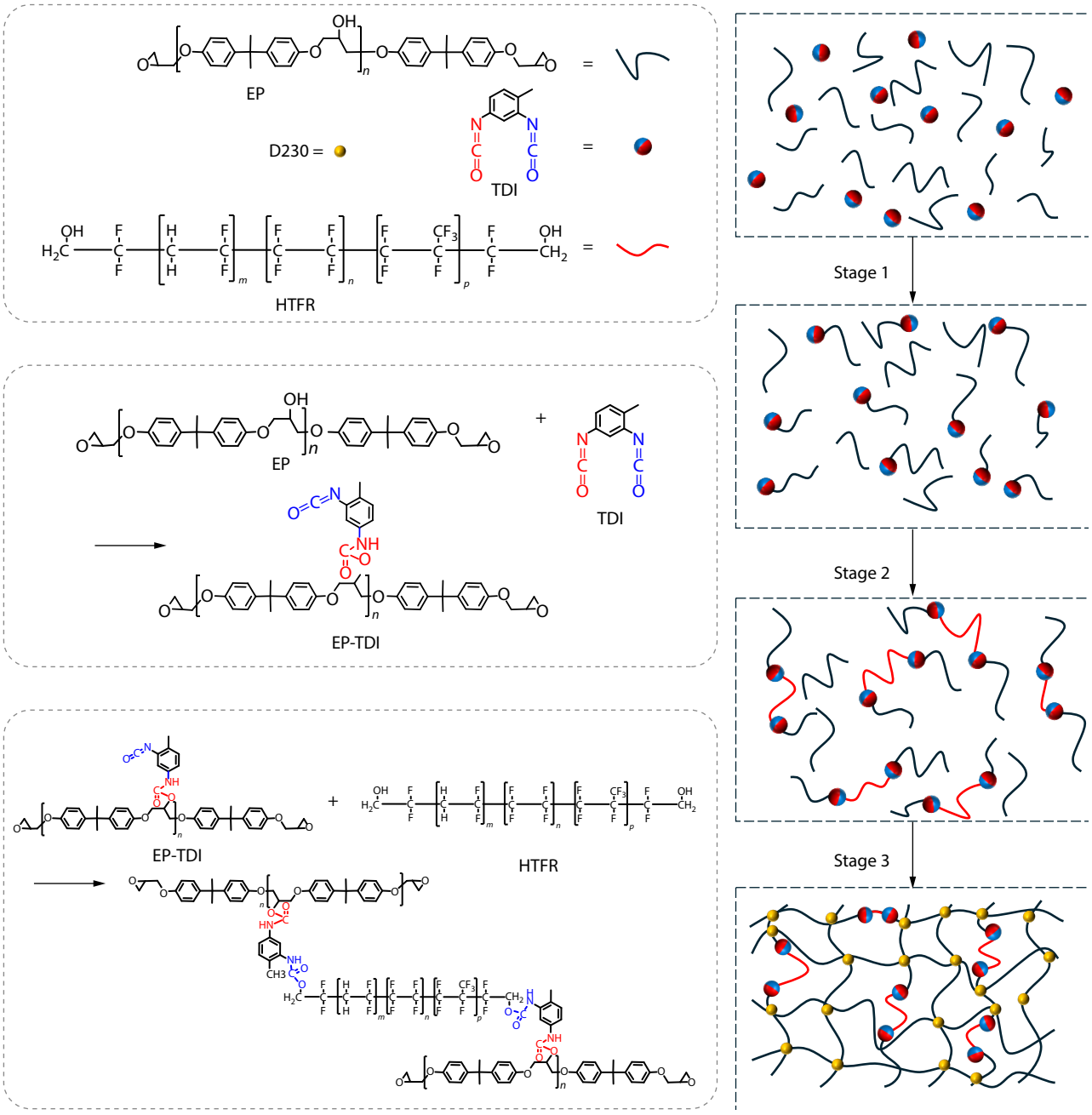

Fig. 9 Schematic illustration of the preparation mechanism for epoxy coatings modified with HTFR.

CONCLUSIONS

The hydrophobicity and toughness results of the coatings modified with HTFR allow for the following conclusions.

(1) The successful grafting of HTFR onto E51 was confirmed by the gradual enhancement of the C=O absorption band at 1731 cm^{-1} and the corresponding reduction of the —NCO absorption band at 2273 cm^{-1}, which indicates that carbamate linkages were formed between the —OH groups of both E51 and HTFR with the —NCO groups of TDI.

(2) With increasing HTFR concentration, the hydrophobic properties, mechanical properties, and cavitation erosion resistance of the modified epoxy coating initially improve and then decrease. The incorporation of HTFR optimized the crosslinked network structure, leading to synergistic enhancement of the overall performance of the coating.

(3) The fracture surface of the unmodified coating was relatively smooth. With an increase in the HTFR content, the fracture surfaces gradually exhibited ductile fracture characteristics. Furthermore, the rubber phase achieves a moderate domain size and uniform distribution within the epoxy matrix, forming an ideal microphase-separated structure.

Conflict of Interests

The authors declare no interest conflict.

https://doi.org/10.1007/s10118-026-3688-4

Data Availability Statement

The data supporting the findings of this study are available from the corresponding author upon reasonable request.

ACKNOWLEDGMENTS

This work was financially supported by the Natural Science Support Program of Xinjiang Production and Construction Corps (XPCC), China (No. 2025YD005), Fundamental Research Funds for the Central Universities, Chang'an University (CHD) (No. 300102314901), Shaanxi Transportation Technology Project, China (No. 24-104K), Project funded by the China Postdoctoral Science Foundation (No. 2024M762772), Shaanxi Province Natural Science Basic Research Program Project (No. 2025JC-YBQN-499), and Young Talent Fund of Xi'an Association for Science and Technology (No. 0959202513004). The authors also thank the reviewers for their valuable comments and suggestions on our manuscript.

REFERENCES

1 Toldy, A.; Szolnoki, B.; Marosi, G. Flame retardancy of fibre-reinforced epoxy resin composites for aerospace applications. *Polym. Degrad. Stabil.* **2011**, *96*, 371–376.
2 Radzuan, N.; Ismail, N.; Radzi, M.; Bin Razak, Z.; Tharizi, I.; Sulong, A.; Haron, C.; Muhamad, N. Kenaf composites for automotive components: enhancement in machinability and moldability. *Polymers* **2019**, *11*, 1707.
3 Xu, Y.; Shan, H.; Liu, Q.; Lin, Y.; Wu, L.; Xu, S.; Ji, J. Deicing performance improvement of single-component polyurethane pavement materials. *J. Mater. Civ. Eng.* **2025**, *37*, 04025389.
4 Yuan, D.; Jiang, W.; Sha, A.; Xiao, J.; Wu, W.; Wang, T. Technology method and functional characteristics of road thermoelectric generator system based on seebeck effect. *Appl. ENERGY* **2023**, *331*, 120459.
5 Jiang, W.; Yuan, D.; Shan, J.; Ye, W.; Lu, H.; Sha, A. Experimental study of the performance of porous ultra-thin asphalt overlay. *Int. J. Pavement Eng.* **2022**, *23*, 2049–2061.
6 Zhang, J.; Zhang, Z.; Huang, R.; Tan, L. Advances in toughening modification methods for epoxy resins: a comprehensive review. *Polymers* **2025**, *17*, 1288.
7 Turkben, M.; Kocaman, S.; Özmeral, N.; Soydal, U.; Cerit, A.; Ahmetli, G. Sustainable production of recycled rubber waste composites with various epoxy systems: a comparative study on mechanical and thermal properties. *Ind. Crops Prod.* **2023**, *195*, 116490.
8 Picu, C.; Krawczyk, K.; Wang, Z.; Pishvazadeh-Moghaddam, H.; Sieberer, M.; Lassnig, A.; Kern, W.; Hadar, A.; Constantinescu, D. Toughening in nanosilica-reinforced epoxy with tunable filler-matrix interface properties. *Compos. Sci. Technol.* **2019**, *183*, 107799.
9 Liu, W.; Ahmad, M.; Song, P.; Fang, Q.; Li, Q.; Huang, G.; Yang, C. In situ synthesis of organic polymer-inorganic nano zno core-shell structured sizing agents and their effect on carbon fiber interfaces and composite properties. *Polymers* **2025**, *17*, 773.
10 Yan, C.; Wang, H.; Song, L.; Zhou, G. Preparation, characterization, and performance of reactive phenolphthalein poly(aryl ether sulfone) toughenners highly compatible with epoxy resin. *J. Appl. Polym. Sci.* **2024**, *141*, e55480.
11 Chen, D.; Li, J.; Yuan, Y.; Gao, C.; Cui, Y.; Li, S.; Wang, H.; Peng, C.; Liu, X.; Wu, Z.; Ye, J. A new strategy to improve the toughness of epoxy thermosets by introducing the thermoplastic epoxy. *Polymer* **2022**, *240*, 124518.
12 Chai, M.; Liu, H.; Wu, Y.; Xue, K.; Zhang, P.; Liu, L.; Huang, Y. Flame retardant, toughened, reinforced, transparent and long shelf-life one-component epoxy resins *via* a p/n/si-containing hyperbranched polymer. *Chem. Eng. J.* **2024**, *493*, 152785.
13 Banan, A.; Mehdipour, H. Controlled degradation and functionalization of natural rubber by ozonolysis in organic solvent. *J. Polym. Res.* **2021**, *28*, 333.
14 Ibrahim, S.; Daik, R.; Abdullah, I. Functionalization of liquid natural rubber *via* oxidative degradation of natural rubber. *Polymers* **2014**, *6*, 2928–2941.
15 Kim, D.; Ahn, B.; Kim, K.; Lee, J.; Kim, I.; Kim, W. Effects of molecular weight of functionalized liquid butadiene rubber as a processing aid on the properties of ssbr/silica compounds. *Polymers* **2021**, *13*, 850.
16 Thomas, R.; Durix, S.; Sinturel, C.; Omonov, T.; Goossens, S.; Groeninckx, G.; Moldenaers, P.; Thomas, S. Cure kinetics, morphology and miscibility of modified DGEBA-based epoxy resin–effects of a liquid rubber inclusion. *Polymer* **2007**, *48*, 1695–1710.
17 Arcos-Casarrubias, J.; Vázquez-Torres, H.; Granados-Olvera, J.; Cedeño, A.; Cervantes-Uc, J. Vscoelastic behavior and toughness of the DGEBA epoxy resin with 1,2-diaminocyclohexane: effect of functionalized poly(dimethylsiloxane), diglycidyl ether, PDMS-DGE, pre-reacted with 1,2-diaminocyclohexane. *Polym. Bull.* **2022**, *79*, 2871–2901.
18 Dou, H.; Tian, B.; Huang, Y.; Quan, Y.; Chen, Q.; Yin, G. Improved mechanical properties of ATBN-toughened epoxy networks by controlling the phase separation scale. *J. Adhes. Sci. Technol.* **2016**, *30*, 642–652.
19 Chen, S.; Wang, T. Hydroxy-terminated liquid nitrile rubber modified castor oil based polyurethane/epoxy ipn composites: damping, thermal and mechanical properties. *Polym. Test.* **2011**, *30*, 726–731.
20 Ge, Z.; Zhang, W.; Huang, C.; Luo, Y. Study on epoxy resin toughened by epoxidized hydroxy-terminated polybutadiene. *Materials* **2018**, *11*, 932.
21 Lou, C.; Zhang, X.; Wang, Y.; Chen, Z.; Li, H. Toughening epoxy resin with blocked isocyanate containing soft chain. *J. Appl. Polym. Sci.* **2015**, *132*, 41345.
22 Tang, W.; Zeng, T.; Hu, J.; Li, J.; Yang, R. Investigation on the thermal decomposition of the elastomer containing fluoroolefin segment by DSC-TG-MS-FTIR. *Polym. Adv. Technol.* **2021**, *32*, 4880–4890.
23 Zhang, X. F.; Cao, T.; Zhao, T. H.; Ma, C.; Liu, P. Y. Preparation and properties of a new type of flexible epoxy resin based on a molecular network structure. *Express Polym. Lett.* **2021**, *15*, 1032–1040.
24 Zhang, X.; Li, P.; Huang, D.; Shi, X.; Shi, Y.; Qu, C.; Tan, Q. Study on a novel epoxy-terminated dendritic modifier as an active toughening agent for epoxy resin. *J. Appl. Polym. Sci.* **2024**, *141*, e55717.
25 Kim, H.-C.; Moon, S.-J.; Kwon, Y.-R.; Moon, S.; Kim, D.; Kim, D.-H. Novel glycidyl carbamate functional epoxy resin using hydroxyl-terminated polybutadiene. *Polymers* **2024**, *16*, 3107.
26 Wu, P.; Li, S.; Guo, H.; Zhang, H.; He, R. Research on electromagnetic and rheological performance of microwave-sensitive emulsified asphalt containing SiC and Fe_3O_4. *Materials* **2025**, *18*, 4283.
27 Fedorov, Y.; Shadrinov, N.; Vasil'ev, S.; Savvina, A. Influence of thermoplastic elastomer filler on impact viscosity of epoxy resin at low temperatures. *Inorg. Mater.-Appl. Res.* **2023**, *14*, 1007–1012.
28 Wu, Y.; Yang, Q.; Zhang, H.; Zhou, Y.; Guo, H.; Wang, Z.; Li, G. Enhancing hydrophobicity and corrosion resistance of epoxy

Graphical Abstract

Improvements of Hydrophobicity and Toughness of Epoxy Coatings Modified with Hydroxyl-terminated Fluororubber

Yu-Tong Zhou, You-Fan Wu, Qian-Qian Yang, Hai-Bao Zhang, Ting Zhang, Hao-Yan Guo, Zhen-Jun Wang, and Gang Li

Chang'an University; Shaanxi Union Research Center of University and Enterprise for Advanced Transportation Infrastructure Materials; Shihezi University

Flexible fluororubber grafting onto epoxy resin achieves high toughness (elongation at break: 46.40%) and hydrophobicity (contact angle: 110°) at 25% HTFR content, significantly enhancing cavitation erosion resistance.

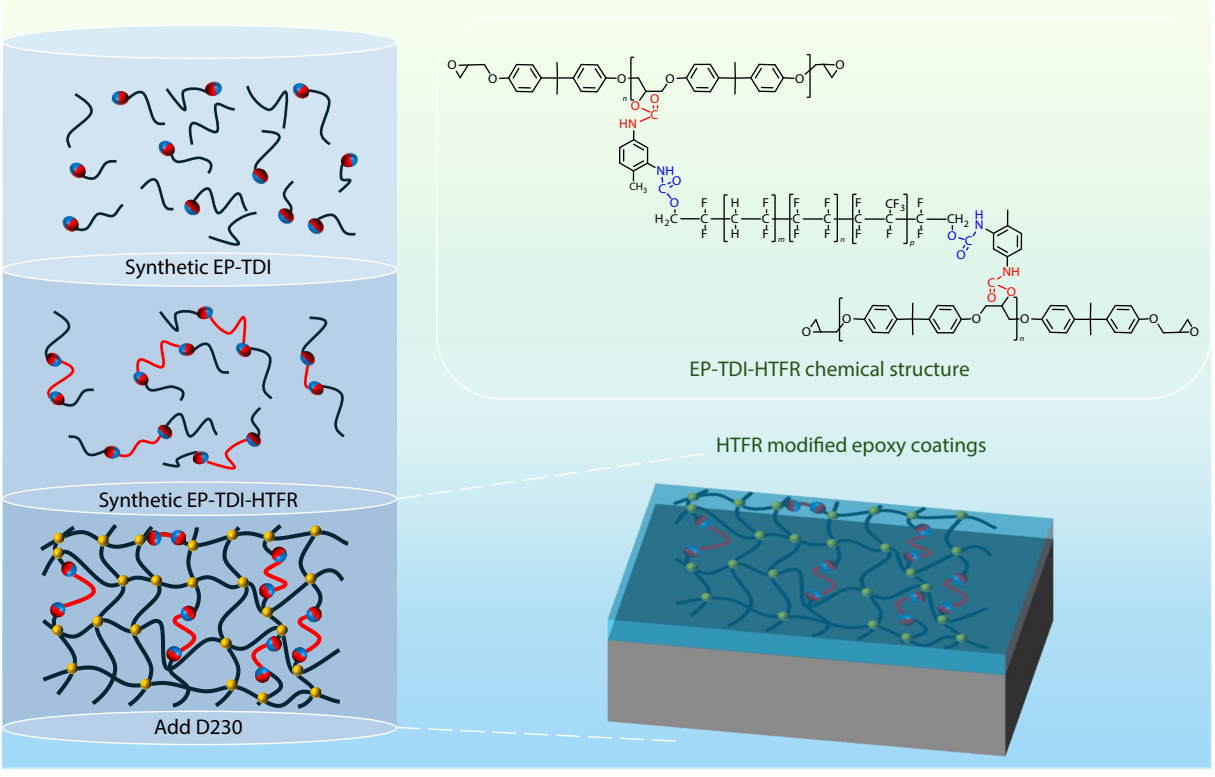

Chinese J. Polym. Sci. 2026, 44, 3129–3141 *https://doi.org/10.1007/s10118-026-3688-4*

resin coatings using KH570-ZrO_2 nanoparticles. *Polym. Test.* **2026**, *154*, 109070

29 Huang, B.; Ai, S.; Tan, J.; Zhou, B.; Pan, Y.; Zheng, Z.; Ding, X.; Deng, J. Enhancing tensile strength, hydrophobicity, and flame retardancy of epoxy resin: π-π stacking and hydrogen bonds, fluorine, and phosphorus-fluorine synergy. *ACS Appl. Eng. Mater.* **2025**, *3*, 2176–2189.

30 Wang, X.; Liao, X.; Tian, J.; Zou, H.; Liu, P. Fluorine-containing main-chain type active esters as curing agents for epoxy resins to achieve superior dielectric and thermal performances. *Prog. Org. Coat.* **2024**, *197*, 108806.

31 Chai, W.; Wang, C.; Liu, H.; Gao, Y.; Zhang, S.; Xin, M.; Wang, R.; Liu, Z.; Wang, H. Novel amphiphilic crosslinked architecture in coatings for enhanced high-voltage corrosion resistance. *Surf. Interfaces* **2025**, 107338.

32 Shi, E.; Liu, B.; Zhao, B.; Jiang, C.; Zhou, W. Preparation and anti-icing characteristics of durable superhydrophobic composite coatings of nano-silica / fluorocarbon resin. *China Surf. Eng.* **2025**, *38*, 244–254.

33 Wang, C.; Yun, T.; You, W.; Ding, Y.; Fan, Z.; Liu, G.; Yu, W.; Yan, X. Mechanical-bond-toughened epoxy resins. *Angew. Chem. Int. Ed.* **2025**, *64*, e202516283.

34 Wang, Y.; Deng, J.; Zhao, J.; Ding, Y.; Yang, L.; Zhang, Z.; Yan, X. Bolstering the mechanical robustness of supramolecular polymer network by mechanical bond. *Chinese J. Polym. Sci.* **2024**, *42*, 1536–1544.

35 Ji, X.; Wang, J.; Wang, Z.; Mao, B.; Cao, Y.; Xie, Y.; Yan, Y. Epoxy-poss toughened phenol-formaldehyde resin adhesive and its enhancement on the interfacial bonding strength of bamboo based composite. *Polym. Compos.* **2025**, *46*, 870–885.

36 Sim, K.; Back, J.; Han, G.; Kim, H. High-performance automotive adhesives with urethane-modified and nanophase-separated

epoxy systems. *Compos. Part Appl. Sci. Manuf.* **2025**, *190*, 108652.
37 Chen, Z.; Li, Z.; Ran, Z.; Zhang, Y.; Lin, F.; Zhou, Y. Study on the performance of composite-modified epoxy resin potting adhesive for repairing oblique cracks. *Materials* **2025**, *18*, 3197.
38 Zhang, H.; Li, Y.; Huan, D.; Li, M.; Yang, L. Study on toughening modification of epoxy resin and its properties of T700 carbon fibre composites. *J. Reinf. Plast. Compos.* **2026**, *45*, 1503–1517..
39 Zhou, Y.; Zhao, Z.; Zeng, Y.; Tian, S.; Sun, F.; Cheng, Y.; Li, Y.; Fu, Z.; Fu, J. Ultra-robust and tough epoxy resin enabled by pulley mechanism-based curing agent for strong and reversible adhesion. *Adv. Funct. Mater.* **2025**, *35*, e17052.
40 Parameswaranpillai, J.; Sanjay, M.; Siengchin, S.; Sidhardhan, S.; Jose, S.; Salim, N.; Hameed, N. Intermolecular hydrogen bonding in developing nanostructured epoxy shape memory thermosets: effects on morphology, thermo-mechanical properties and surface wetting. *Polym. Test.* **2020**, *81*, 106279.
41 Li, D.; Yu, L.; Ning, S.; Li, P.; Chen, C.; Zhao, D.; Liao, M.; Meng, Q.; Zhang, S.; Fang, Q.; Kang, H.; Li, L.; Yang, J. Upcycling of waste fluororubber to photocurable high-performance vinyl-terminated liquid fluororubber by multifield coupling one-pot stepwise reactions. *Adv. Sci.* **2025**, *12*, e01460.
42 Karami, M.; Kalaee, M.; Khajavi, R.; Moradi, O.; Zaarei, D. Thermal degradation kinetics of epoxy resin modified with elastomeric nanoparticles. *Adv. Compos. Hybrid Mater.* **2022**, *5*, 390–401.
43 Ruamcharoen P, Umaree S, Ruamcharoen J. Relationship between tensile properties and morphology of epoxy resin modified by epoxidised natural rubber. *J. Mater. Sci. Eng.* **2011**, *5*, 504–510.
44 Lou, C.; Liu, X. Functional dendritic curing agent for epoxy resin: processing, mechanical performance and curing/toughening mechanism. *Compos. Part B Eng.* **2018**, *136*, 20–27.
45 Tian, W.; Wang, S.; Wang, C.; Xu, H.; Zhao, Y.; Jin, H.; Tian, L. An epoxy-modified polyurethane composite coating with repetitive self-healing function for anti-cavitation, anticorrosion, and antifouling applications. *Chem. Eng. J.* **2023**, *477*, 146849.
46 Zhang, Z.; Hou, G.; Wan, H.; Ma, J.; Ye, Y.; Zhou, H.; Chen, J. Effect of epoxy resin modification on the cavitation erosion resistance of polyamide-imide coatings. *China Surf. Eng.* **2024**, *37*, 88–101.
47 Tian, W.; Guo, Z.; Wang, S.; Yu, H.; Wang, S.; Jin, H.; Tian, L. Hydrogen and DA bond-based self-healing epoxy-modified polyurea composite coating with anti-cavitation, anticorrosion, antifouling, and strong adhesion properties. *J. Mater. Sci. Technol.* **2024**, *187*, 1–14.
48 Ogawa, M.; Morimura, A.; Haba, I.; Yonezu, A. Coarse-grained molecular dynamics simulations of nano-deformation behavior of epoxy adhesives' interface during atomic force microscopy (AFM) mechanical testing. *Polymer* **2025**, *320*, 128071.
49 Wu, Y.; Zhou, Y.; Zhang, H.; Yang, Q.; Zhang, T.; Guo, H.; Wang, Z. Mechanical properties and hydrophobicity improvement of epoxy coatings through synthesis of modified alicyclic amine. *Polymer* **2025**, *341*, 129298.
50 Din, I.; Bathusha, M.; Khan, K. Effects of liquid rubber-modified epoxy on the fracture toughness of rGO-Coated fabric piezoresistive composites. *Compos. Commun.* **2025**, *56*, 102368.
51 Zhou, H.; Shi, Z.; Zhou, X.; Li, X.; Wen, Y.; Xue, Z.; Wang, Y.; Xie, X. Reversible and ultrastrong epoxy-polyurethane adhesives with microphase separation. *Adv. Funct. Mater.* **2025**, *35*, 2506419.
52 Wang, S.; Yu, Z.; Sun, X.; Panahi-Sarmad, M.; Yang, P.; Zhu, P.; Zhu, Y.; Liu, H.; Jiang, F. A Universal strategy to mitigate microphase separation *via* cellulose nanocrystal hydration in fabricating strong, tough, and fatigue-resistant hydrogels. *Adv. Mater.* **2025**, *37*, 2416916.
53 Fernandez-Rico, C.; Schreiber, S.; Oudich, H.; Lorenz, C.; Sicher, A.; Sai, T.; Bauernfeind, V.; Heyden, S.; Carrara, P.; De Lorenzis, L.; Style, R.; Dufresne, E. Elastic microphase separation produces robust bicontinuous materials. *Nat. Mater.* **2024**, *23*, 124.
54 Carrara, A.; Rodrigues, V.; Dutra, R.; Dutra, J. Impact assessment of synthesis parameter stirring speed in final physicochemical properties of PU microcapsules incorporated into epoxy matrixes. *An. Acad. Bras. Cienc.* **2023**, *95*, e20201518.

https://doi.org/10.1007/s10118-026-3688-4